Cell

Molecular Anatomy of a Trafficking Organelle

Shigeo Takamori,[1,13] Matthew Holt,[1] Katinka Stenius,[7,14] Edward A. Lemke,[2] Mads Grønborg,[1,4] Dietmar Riedel,[3] Henning Urlaub,[4] Stephan Schenck,[1,13] Britta Brügger,[8] Philippe Ringler,[9] Shirley A. Müller,[9] Burkhard Rammner,[10] Frauke Gräter,[5] Jochen S. Hub,[5] Bert L. De Groot,[5] Gottfried Mieskes,[1] Yoshinori Moriyama,[11] Jürgen Klingauf,[2] Helmut Grubmüller,[6] John Heuser,[12] Felix Wieland,[8] and Reinhard Jahn[1,*]

[1] Department of Neurobiology
[2] Department of Membrane Biophysics
[3] Laboratory of Electron Microscopy
[4] Laboratory of Bioanalytical Mass Spectrometry
[5] Laboratory of Biomolecular Dynamics
[6] Department of Theoretical and Computational Biophysics
Max-Planck Institute for Biophysical Chemistry, 37077 Göttingen, Germany
[7] Department of Cell Biology, Yale University School of Medicine, New Haven, CT 06510, USA
[8] Department of Biochemistry, University of Heidelberg, 69120 Heidelberg, Germany
[9] M.E. Müller Institute, Biozentrum, University of Basel, CH-4056 Basel, Switzerland
[10] Scimotion, Harkortstrasse 121, 22765 Hamburg, Germany
[11] Laboratory of Membrane Biochemistry, Okayama University Graduate School of Medicine, Dentistry and Pharmaceutical Science, Okayama 700-8530, Japan
[12] Department of Cell Biology, Washington University, St. Louis, MO 63110, USA
[13] Present address: 21st Century COE Program, Department of Neurology and Neurological Science, Graduate School of Medicine, Tokyo Medical and Dental University, Tokyo 113-8519, Japan.
[14] Present address: 31 Surry Road, Arlington, MA 02476, USA.
*Contact: rjahn@gwdg.de
DOI 10.1016/j.cell.2006.10.030

SUMMARY

Membrane traffic in eukaryotic cells involves transport of vesicles that bud from a donor compartment and fuse with an acceptor compartment. Common principles of budding and fusion have emerged, and many of the proteins involved in these events are now known. However, a detailed picture of an entire trafficking organelle is not yet available. Using synaptic vesicles as a model, we have now determined the protein and lipid composition; measured vesicle size, density, and mass; calculated the average protein and lipid mass per vesicle; and determined the copy number of more than a dozen major constituents. A model has been constructed that integrates all quantitative data and includes structural models of abundant proteins. Synaptic vesicles are dominated by proteins, possess a surprising diversity of trafficking proteins, and, with the exception of the V-ATPase that is present in only one to two copies, contain numerous copies of proteins essential for membrane traffic and neurotransmitter uptake.

INTRODUCTION

Eukaryotic cells are compartmentalized into membrane-bound organelles that communicate with each other by membrane trafficking. While many organelles readily undergo fusion or fission, transport between different organelles usually involves specialized trafficking vesicles. These vesicles bud from the precursor compartment and are transported to the target compartment, where they dock and fuse. Trafficking vesicles deliver both membrane constituents and soluble content material from the donor to the acceptor compartment or to the extracellular space (Bonifacino and Glick, 2004).

Small trafficking vesicles, with diameters ranging between 40 and 80 nm, can be considered as the basic minimal units of membrane traffic. Vesicle transport, target recognition, docking, and fusion each involve the ordered and sequential recruitment of protein complexes from the cytoplasm. The membrane constituents of the organelle are ultimately responsible for orchestrating association of the complex, task execution, and complex disassembly. In recent years, many of the proteins involved in these reactions have been identified (Bonifacino and Glick, 2004). However, little is known about overall membrane structure, including the concentration of integral membrane and membrane-associated proteins, or about the surface density of trafficking proteins such as SNAREs and Rabs.

In the present study, we have attempted to arrive at a comprehensive and quantitative molecular description of synaptic vesicles (SVs) as model trafficking organelles. SVs are concentrated in the presynaptic nerve terminals of every neuron. They store neurotransmitters and undergo Ca^{2+}-dependent exocytosis upon the arrival of an action potential. After exocytosis, SVs are retrieved by clathrin-dependent endocytosis and are locally recycled to regenerate exocytosis-competent vesicles. Although the intermediate steps in the recycling pathway are still debated, it is clear that nerve terminals contain endosomes and that the SV cycle may involve endosomal intermediates, although not necessarily during each recycling event (Südhof, 2004).

SVs can be purified to apparent homogeneity in large quantities, making them amenable to biochemical studies (Nagy et al., 1976; Huttner et al., 1983). Indeed, the protein composition of SVs is, at present, better understood than that of any other trafficking organelle, and several proteins first identified in SVs turned out to be founding members of conserved protein families involved in all trafficking steps (Jahn and Südhof, 1994). In addition, SVs contain the machinery required for the uptake and storage of neurotransmitters including vesicular transporters, ion channels, and the vacuolar H^+ ATPase that fuels the transporters (Ahnert-Hilger et al., 2003). Recently, proteome analyses of enriched fractions of both SVs and brain-derived clathrin-coated vesicles have been performed, resulting in the identification of many of the known vesicle proteins (Morciano et al., 2005; Blondeau et al., 2004; see also Discussion).

In contrast to our advanced knowledge about individual SV proteins, we lack even elementary quantitative information on the composition of the whole vesicle. With a diameter of approximately 40 nm, SVs are small organelles, making them comparable in complexity to other supramolecular structures such as ribosomes, spliceosomes, or viruses. On the other hand, SVs are "dirty" nanostructures that may not have a fixed stoichiometric composition and are constantly visited by cytoplasmic factors. With these caveats in mind, we have used a purified SV fraction from rat brain as the starting point for the description of a prototypic SV, resulting in a detailed (albeit averaged) structural model of this trafficking organelle.

RESULTS

Protein and Lipid Composition of SVs

To obtain a highly purified fraction of SVs, we relied on the modified version (Huttner et al., 1983) of a classical fractionation protocol originally developed by Whittaker and coworkers (Nagy et al., 1976). SVs purified by this procedure are morphologically homogeneous, and more than 95% of them carry major SV proteins such as synaptophysin and synaptobrevin (Jahn and Südhof, 1994).

The protein composition of purified vesicles was analyzed by mass spectrometry (MS) following separation by 16-BAC/SDS-PAGE (Hartinger et al., 1996) as well as by 1D SDS-PAGE. In total, 410 different proteins were unambiguously identified. To compensate at least in part for the nonquantitative nature of the proteomics analysis, we monitored the distribution of 85 proteins (including some that were not found in the proteomics analysis) using immunoblotting of subcellular fractions. This allowed the definition of three major categories: (1) copurification with SVs, (2) ubiquitous distribution in all membrane fractions, and (3) separation away from the vesicle fraction (see Figure S1 in the Supplemental Data available with this article online). The main results are summarized in Table 1; the immunoblot profiles and a list of all the proteins identified by MS are shown in Figures S1 and S3 and Table S1.

More than 80 different integral membrane proteins were identified by proteomics. Of these, approximately 40 are known SV residents. The few known SV membrane proteins missed included SVOP (Janz et al., 1998), the chloride channels ClC3 and ClC7 (Stobrawa et al., 2001), the vesicular neurotransmitter transporters known to be confined to minor SV subpopulations (VMATs and VAChT), and a few SNAREs (see Table 1), resulting in an overall coverage of approximately 80% of all known vesicle membrane proteins. Most of the remaining membrane proteins are residents of the plasma membrane, including some channels, transporters, and a group of adhesion molecules belonging to the IgG superfamily. While the degree of plasma membrane contamination within the SV fraction is known to be low (Walch-Solimena et al., 1995), it is conceivable that some of these proteins may use SVs as part of their recycling pathway. Only a few membrane proteins from other subcellular membranes were identified, confirming that the analyzed SV fraction was of high purity. Some peptides corresponding to open reading frames containing predicted transmembrane segments were detected. Two of the predicted proteins resemble transporters, whereas the others show no homology to known proteins (see Table S1 for more details).

While we expected trafficking proteins to occupy the dominant position in the SV proteome, we were surprised by their diversity. In addition to the SNARE proteins synaptobrevin/VAMP2, syntaxin 1, and SNAP-25, which are known to function in exocytosis, a total of 20 different SNAREs were identified (Table 1), including a novel SNARE with similarities to SNAP-29 (termed SNAP-47; Holt et al., 2006). Of these, 13 copurified with SVs. Thus, SVs are equipped with SNAREs functioning not only in exocytosis but also in other fusion steps such as early and late endosome fusion, supporting the view that SVs communicate with endosomal intermediates at least at some point in their life cycle. Even more surprising was the multitude of Rab proteins identified: 33 in all, more than half of the rat's genetic inventory (Bock et al., 2001). Rabs are presently considered to be the most specific organelle "markers." At present, we cannot exclude that, at least to a certain extent, Rabs are deposited on the vesicles during purification from a GDI-bound soluble

Table 1. Summary of Proteins Identified in Purified SVs

	Method of Detection	Distribution
Trafficking Proteins		
SNAREs		
Synaptobrevin/VAMP1	MS	●
Synaptobrevin/VAMP2	MS	●
Cellubrevin	MS	●
VAMP4	—	●
VAMP7	MS	
Sec22-like1	MS	▽
SNAP-23	—	▽
SNAP-25	MS	▽
SNAP-29	MS	●
SNAP-47	MS	●
Syntaxin 1A	MS	▽
Syntaxin 1B2	MS	▽
Syntaxin 2	—	▽
Syntaxin 3	—	▽
Syntaxin 6	MS	●
Syntaxin 7	MS	●
Syntaxin 13	MS	●
Syntaxin 16b	MS	●
vti1a	MS	●[b]
Tomosyn (b, m)	MS	●
Amisyn	—	▽
Endocytosis-Related Proteins		
AP-1β1	MS	
AP-2 (α1, α2, β1, μ1, σ1)	MS	
AP-3 (δ1, μ2, σ2)	MS	
AP-2 associated kinase 1	MS	
Dynamin 1	MS	▽
Dynamin (2, 3)	MS	
Flotillin 1	MS	
Sorting nexin-5	MS	
Synaptojanin 1	MS	▽
PI-binding clathrin assembly protein	MS	
Small GTPases and Related Proteins[a]		
Rab1	MS	▽
Rab2	MS	
Rab2b	MS	
Rab3A	MS	●
Rab3b	MS	●

Table 1. *Continued*

	Method of Detection	Distribution
Rab3C	MS	●[c]
Rab4 (a, b)	MS	
Rab5 (a–c)	MS	●
Rab6b	MS	
Rab7	MS	●
Rab8 (a, b)	MS	
Rab9b	MS	
Rab10	MS	
Rab11b	MS	●[d]
Rab12	MS	
Rab14	MS	
Rab15	MS	
Rab16	MS	
Rab18	MS	
Rab21	MS	
Rab24	MS	
Rab25	MS	
Rab26	MS	
Rab27b	MS	
Rab30	MS	
Rab31	MS	
Rab33 (a, b)	MS	
Rab35	MS	
Arl10 (b, c)	MS	
RalA	MS	
Rabphilin 3A	MS	●
rap2A-like	MS	
Rap2b	MS	
c-K-ras2	MS	
Di-ras2	MS	
Arfaptin 2	MS	
Arhgap1	MS	
GAP1-like	MS	
Rac1	MS	
RhoB	MS	
Other Trafficking and SV Membrane Proteins		
Synapsin 1	MS	●
Synapsins (2, 3)	MS	
Synaptophysins (1, 2)	MS	●
Synaptogyrins (1, 3)	MS	●

(*Continued on next page*)

Table 1. *Continued*

	Method of Detection	Distribution
SCAMP1	MS	●
SCAMP (3, 5)	MS	
Synaptotagmin 1	MS	●
Synaptotagmins (2, 5, 12, 17)	MS	
Munc-18	MS	▽
Vps33b	MS	
Vps45	MS	▽
Rsec6/8 p71	MS	
Snapin	—	▽
NSF	MS	▽
VAP-33	MS	
CSP	MS	
TRAPPC1	MS	
TRAPPC3	MS	
TRAPPC5	MS	
Bassoon	MS	
Doc2b	MS	
Lamp-1	MS	
MAL2 proteolipid protein	MS	
Piccolo	MS	
rSec8	MS	
β-SNAP	MS	○
Reticulon 1	MS	
SNAP-25-interacting protein	MS	
Pantophysin	MS	
tmp-21 (transmembrane protein)	MS	
TRS85 homolog	MS	
Wfs1	MS	
Transporter and Channel Proteins		
VGLUT1	MS	●
VGLUT2	MS	●
VGLUT3	MS	●
VGAT	MS	●
VAChT	—	●[e]
VMAT2	—	●[e]
V-ATPase: Vo-a	MS	●
V1-A	—	●
V1-B	MS	●
Vo (a1, a4, c, d1)	MS	

Table 1. *Continued*

	Method of Detection	Distribution
V1 (B1, B2, C1, D, E1, F, G1, G2, H)	MS	
Aminophospholipid transporter	MS	●
Proline transporter	MS	
ZnT-3	MS	
Na^+-dependent glucose transporter 1	MS	
GLT-1	MS	○
H^+/myo-inositol cotransporter	MS	
NTT4	MS	
VAT-1 homolog	MS	
Na/K-ATPase	MS	○[f]
F1-ATPase α1	MS	
V-ATPase Ac45	MS	
V-ATPase ap2	MS	
SERCA2a	MS	
Ca-ATPase (1, 2)	MS	
Na/K-ATPase (a1, a2, a3, β1)	MS	
CAT7A14	MS	
SV2 (a-c)	MS	●
Glycoprotein m6a	MS	
Voltage-gated K^+ channel	MS	
VDAC-1	MS	
VDAC-2	MS	
K^+-dependent Na/Ca exchanger	MS	
Na/Ca exchanger 2	MS	
Cytoskeletal Proteins		
Tubulin α	MS	▽
Tubulin (α1, α4, β2, β5)	MS	
Actin (α1, β)	MS	
F-actin capping protein (α2, β)	MS	
ARP 2/3 (1A, 2, 3, 4, 5, 5-like)	MS	●
arp (2, 3, 3β)	MS	
Dynein (lc2, hc1)	MS	
Dynactin 1	MS	
MAP (1A, 6)	MS	
α-internexin	MS	

Table 1. *Continued*

	Method of Detection	Distribution
Kinesin (5A, 5B)	MS	
Septin 7	MS	
Tubulin polymerization-promoting protein	MS	
Myosin (Va, VIIb)	MS	
Cell-Surface Proteins		
MRC OX-2	MS	
Basigin	MS	
Cadherin 13	MS	
Contactin 1	MS	
Contactin-associated protein 1	MS	
Brain link protein 2	MS	
LSAMP	MS	
N-CAM (1, 2)	MS	
Neurofascin	MS	
OBCAM	MS	
Neuronal growth regulator 1	MS	
Neurotrimin	MS	
Stromal cell-derived factor receptor 1	MS	
Thy1 theta	MS	
Immunoglobulin superfamily 4B	MS	
Intercellular adhesion molecule 5 precursor	MS	
MBP (1, 2, 4, 5)	MS	
Myelin-associated glycoprotein	MS	
Myelin proteolipid	MS	
PLP	MS	
Signaling Proteins		
CaMK II (α, β, γ)	MS	
Casein kinase 1ε	MS	
PK-C (β, γ)	MS	
PP1H	MS	
PTP 23	MS	
PTP 9	MS	
R-PTP N polypeptide 2	MS	
R-PTP-ε	MS	
pp60-c-src	MS	
Gα (13, o, i2, q, z)	MS	

Table 1. *Continued*

	Method of Detection	Distribution
Gβ (1, 2, 3, 4)	MS	
IP3 receptor	MS	
PI4K a	MS	
PI4K IIa	MS	
PI3K subunit 4	MS	
Phospholipase D3	MS	
S100 β	MS	

Proteins are classified according to their distribution during subcellular fractionation. Proteins marked ● copurify with SVs (with particular enrichment during the final purification steps); proteins marked ▽ are ubiquitously distributed on subcellular membranes, i.e., present on SVs but not enriched relative to other fractions; proteins marked ○ are lost during the final purification steps and are thus regarded as contaminants (see Figure S1 for examples; a complete set of all blots is provided in Figure S3). MS = proteins identified by mass spectrometry (a complete list is given in Table S1); (—) = proteins not identified by mass spectrometry.

[a] Isoforms distinguished only when indicated.
[b] Data from Antonin et al. (2000).
[c] Data from Fischer von Mollard et al. (1994a).
[d] Data from Khvotchev et al. (2003).
[e] Data from Takamori et al. (2000b).
[f] Data from Walch-Solimena et al. (1995).

pool, although it is commonly believed that membrane binding is compartment specific and involves Rab-specific catalysts (Pfeffer and Aivazian, 2004). Furthermore, some of the Rabs, e.g., Rab1, may reside on contaminating small trafficking vesicles of different origin. However, at least some Rabs are synaptically localized and/or copurify with SVs. These include Rab3a, Rab3b, Rab3c (Schlüter et al., 2002), Rab5 (Fischer von Mollard et al., 1994b; de Hoop et al., 1994), Rab7 (G. Fischer von Mollard and R.J., unpublished data), and Rab11 (Khvotchev et al., 2003).

Our preparation also contained proteins involved in clathrin-mediated endocytosis, in particular, the components of the AP-2 complex (Table 1). This is not surprising, considering that SVs recycle via clathrin-coated vesicles. Furthermore, partially decoated vesicles derived from recycling SVs cofractionate with SVs (Maycox et al., 1992), and many SV proteins were detected in a recent proteome analysis of brain clathrin-coated vesicles (Blondeau et al., 2004).

A large number of peripheral proteins were also identified. These include (1) proteins involved in signaling pathways such as trimeric GTPases, protein and polyphosphoinositide kinases, and phosphatases; (2) cytoskeleton proteins; (3) metabolic enzymes; and (4) chaperones. While some of these proteins may participate in SV function, such as trimeric GTPases (regulation of vesicular

neurotransmitter uptake; Ahnert-Hilger et al., 2003) and cytoskeletal proteins (vesicle transport), others may be only loosely associated with the vesicle membrane, and many are probably contaminants. Finally, we also detected some ribosomal proteins, together with proteins involved in RNA processing and proteasome components. Both ribosomes and proteasomes are in the same size range as SVs and thus are expected to copurify to some extent.

Next, we performed quantitative determinations of more than a dozen major SV proteins. Quantitation was performed by either western blotting or dot blotting, using purified proteins as standards. Figure 1A shows an example of such a determination, and Figure 1B summarizes the results for all analyzed proteins, including a few data from previous publications. Synaptophysin, synaptobrevin 2 (also referred to as VAMP2), synaptotagmin 1, and synapsin I are among the most abundant proteins, in very good agreement with earlier results (Goelz et al., 1981; Walch-Solimena et al., 1995). We also included two vesicular glutamate transporters, VGLUT1 and VGLUT2, in our analysis. These transporters display a differential localization in the brain and are known to reside on nonoverlapping vesicle subpopulations (Fremeau et al., 2001). To estimate their relative contribution, we performed immunogold labeling on purified vesicles. VGLUT1 antibodies and VGLUT2 antibodies labeled 66.8% and 23.3% of the vesicles, respectively. Immunogold labeling of synaptophysin, used as a reference, labeled more than 97% of all membranous structures (data not shown). In summary, the proteins quantified here account for approximately 45% (VGLUT1-positive vesicles) and 48% (VGLUT2-positive vesicles) of the total vesicle protein.

The lipid composition was measured by electrospray ionization (ESI) coupled with collision-induced dissociation (CID) and mass spectrometry (Brügger et al., 1997). Except for cholesterol, the overall composition (Figures 1C and 1D) agrees approximately with older measurements involving thin-layer chromatography (Nagy et al., 1976; Benfenati et al., 1989). It is interesting to note that (1) the cholesterol content (40 mol%) is high, (2) the amount of phosphatidylinositol is very low (as noted previously; Benfenati et al., 1989), and (3) there is a high proportion of the plasmalogen form of phosphatidylethanolamine.

Quantitative Analysis of Physical Parameters

All data described so far were derived from highly purified vesicle fractions and involved bulk measurements made on an unknown number of vesicles. However, to construct a molecular model, the physical parameters of an average SV need to be determined.

The number of SVs present was measured by fluorescence correlation spectroscopy (FCS), which is a reliable standard way of counting particles in solution (Magde et al., 1972; Muller et al., 2003). Vesicles were labeled with the membrane dye FM1-43, which only becomes fluorescent upon membrane insertion. Addition of vesicles to buffer containing FM1-43 increased the emitted light intensity severalfold (Figure 2A). A strong time-dependent autocorrelation (Figure 2B, bottom, black lines) for fluctuations in the signal (Figure 2B, top) was observable, which was only seen when vesicles were added (Figure 2B, bottom, red line). For each sample, the protein concentration was determined in parallel. Based on the FCS counts, the following average values were then calculated for single vesicles: protein = (17.1 ± 0.19) × 10^{-18} g/vesicle (Figure 2C), phospholipids = 8.8 × 10^{-18} g/vesicle, and cholesterol = 3.7 × 10^{-18} g/vesicle, resulting in a total predicted dry mass of 29.6 × 10^{-18} g/vesicle (Table 2; see also Supplemental Data).

Two independent approaches were used to confirm the mass of single vesicles. First, we measured vesicle volume and density to directly calculate the average mass of hydrated and solution-filled vesicles. Equilibrium density-gradient centrifugation in iodixanol (OptiPrep) was used to determine the buoyant density, resulting in an average density of 1.10 g/ml (Figure 3A). To measure vesicle volume, we employed cryoelectron microscopy of shock-frozen and unstained vesicle samples imaged directly in vitrified ice. Figure 3B shows the histogram of such measurements from 790 vesicles, giving an average diameter of 45.18 nm when all vesicles were included in the analysis and 41.6 ± 8.4 (SD) nm as an average when a few large profiles were eliminated (including only diameters between 30 nm and 56 nm). These measurements are well within the range reported previously from fixed and stained brain sections (Harris and Sultan, 1995). A mass/diameter correlation can now be established, which, after correcting for the SV water content, allows for the calculation of the dry mass (Figure 3C; see legend for details). A diameter of 41.6 nm would yield a dry mass of 22 × 10^{-18} g/vesicle, but the volume contribution of the surface proteins is not taken into account. Although this volume could not be directly determined, we assume that it adds, on average, at least 1 nm to the radius measured to the lipid surface. Indeed, a dry mass of ~30 × 10^{-18} g/vesicle would result in a vesicle diameter of ~44 nm, i.e., a radius increase of 1.2 nm. Thus, the estimate of the total dry mass obtained by this method is well within the range obtained by bulk protein and lipid measurements and vesicle counting.

A second estimate of the vesicle mass distribution was obtained by quantitative dark-field scanning transmission electron microscopy (STEM) (Engel, 1978). An average mass 16.2 ± 4.1 MDa (n = 281) or 15.9 ± 3.5 MDa (n = 276, excluding a few very high values) was determined (Figure 3D). The latter corresponds to (26.4 ± 5.8) × 10^{-18} g/vesicle, in good agreement with the predicted dry mass of 29.6 × 10^{-18} g/vesicle (see Figure S5 for details).

Construction of a Molecular Model

To construct a molecular model of a prototypic SV, we first calculated the average copy number per vesicle of the proteins quantified above (see Figure 1) based on the known molecular mass, Avogadro's number, and the average protein content per vesicle (Table 2; see also Table S2).

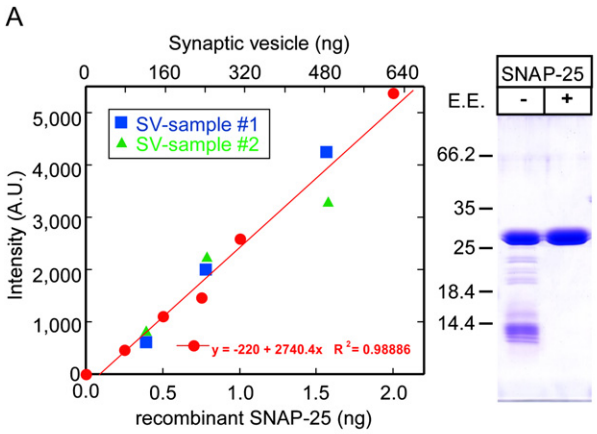

B

Protein	% of total SV proteins
Synaptophysin	10.20 ± 1.54[1,4]
Synaptobrevin 2	8.60 ± 1.55[1]
Syntaxin 1	2.00 ± 0.27[1,5]
SNAP25	0.40 ± 0.06[1,6]
Synapsins	6[2,3]
Rab3A	2.5[2]
Synaptotagmin 1	7[3]
Synaptogyrin 1	0.5[2]
SV2	1.4[2]
SCAMP	0.3[2]
CSP	0.6[2]
VGLUT1	5.36 ± 1.11[1,7]
VGLUT2	9.01 ± 2.31[1,7]
V-ATPase V1-B subunit	1.15 ± 0.21[1]

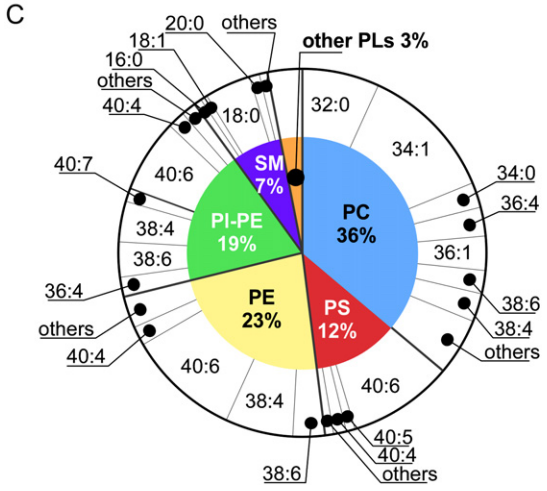

D

Membrane lipid	ng lipid/µg protein
Phosphatidylcholine	186 ± 37
Phosphatidylethanolamine	
1- ester	120 ± 18
1- ether (plasmalogen)	96 ± 14
Phosphatidylserine	68 ± 7.2
Phosphatidylinositol	9.73 - 10*
Sphingomyelin	37 ± 5.1
Cholesterol	215 ± 25
Hexylceramide	8.6 ± 4.0
Ceramide	1.2 ± 0.1
Protein : Phospholipid (w/w)	1.94 ± 0.23

Figure 1. Quantitative Measurements of SV Proteins and Lipids

(A) Left panel: Determination of the amount of SNAP-25 using quantitative western blotting of vesicle proteins in comparison to a standard curve of purified recombinant protein. All measurements within the linear range of the standard curve (0.0–2.0 ng for SNAP-25, red circles) were taken into account. Densitometric measurements from two independent SV samples (SV sample #1, blue squares; SV sample #2, green triangles) are shown (left panel). Right panel: Three micrograms of SNAP-25 standard proteins purified conventionally (left lane) and after an additional electroelution step (right lane) was subjected to SDS-PAGE followed by Coomassie blue staining.

(B) Quantities of major SV proteins. For each protein, the values are expressed as % of the specific protein related to the total SV protein. Superscripted 1 denotes data determined according to the procedure shown in (A). Superscripted 2 denotes data determined by quantitative dot blotting (Jahn et al., 1984) using purified recombinant proteins (mostly containing affinity tags) as a standard. Superscripted 3 denotes data from Chapman and Jahn (1994). Superscripted 4 denotes data for which somewhat lower values were previously reported (Navone et al., 1986). Superscripted 5 denotes values similar to those published earlier (Goelz et al., 1981; Walch-Solimena et al., 1995). Superscripted 6 denotes values lower than those published earlier by our laboratory (Walch-Solimena et al., 1995). Superscripted 7 denotes values corrected for the percentage of vesicles positive for these transporters, which was determined by immunogold labeling of negatively stained vesicle fractions.

(C and D) Quantitative analysis of lipid constituents.

(C) A pie diagram depicts the mol% of the various phospholipid species and the fatty-acid distribution.

(D) Values expressed per µg of protein. Five samples were analyzed in triplicate. The average and standard deviation are given. Asterisk indicates that only two samples were analyzed; numbers indicate range of values.

According to these data, a typical SV contains 70 synaptobrevins, 32 synaptophysins, between 9 and 14 neurotransmitter transporters, 10 Rab3As, 8 synapsins, and 15 synaptotagmin 1s. Thus, the proteins currently known to be essential for both exocytosis and neurotransmitter loading are present in high copy numbers. Since only the dominant isoform was measured for most proteins, including synaptophysin, synaptotagmin, synaptobrevin, and SV2, the copy number of each protein class is somewhat higher. The only exception is the vacuolar H^+ ATPase, for which an average copy number, 0.7, was obtained. However, this estimate is less certain since we

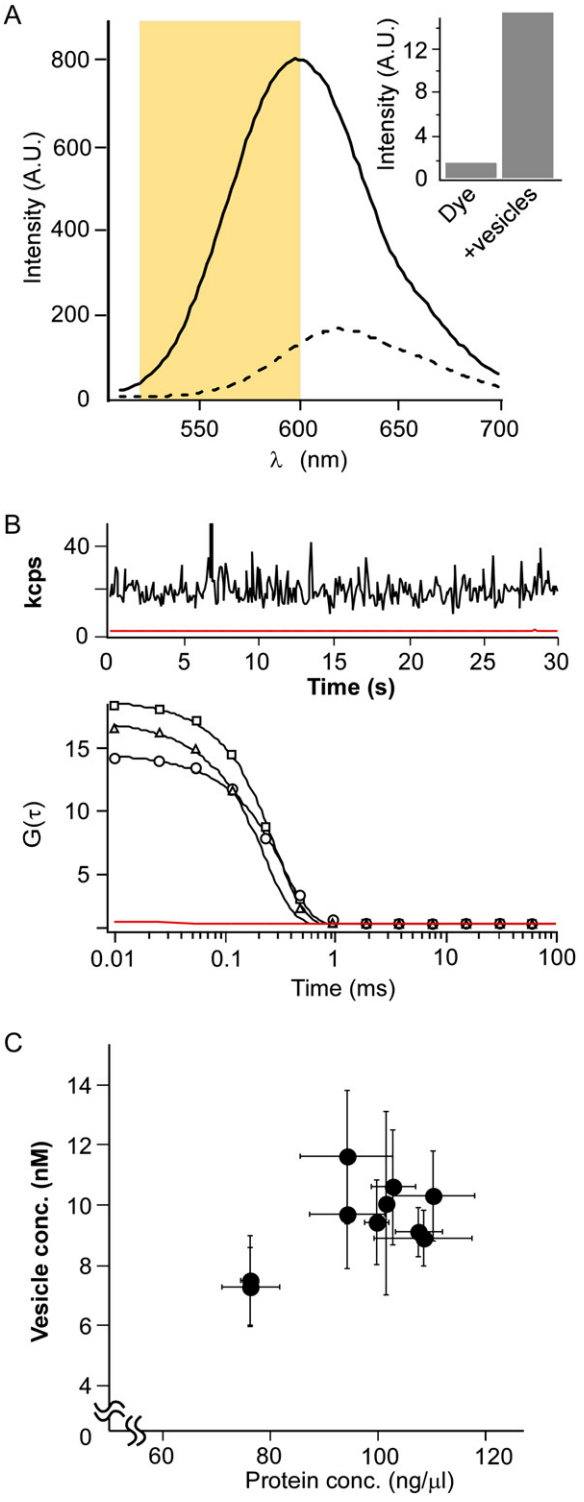

Figure 2. Determination of SV Concentration by Fluorescence Correlation Spectroscopy

(A) Spectra of FM1-43 with and without the addition of SVs to the sample. 2.4 ml of 300 mM glycine, 4 mM HEPES-NaOH (pH 7.4) containing 10 μM FM1-43 was mixed with 300 μl of the purified SV sample. The spectrum of FM1-43 in the sampling buffer (dashed line) shifted slightly to shorter wavelengths upon addition of SVs (solid line). Evaluation of the integral under the spectrum between 520 and 600 nm (yellow box, corresponding to the band-pass filter used in the FCS measurements) revealed that the intensity increased more than 7-fold upon addition of SVs (inset).

(B) Measurement of SV concentration by FCS. In the concentration measurements, the sample was stirred, which does not change the signal amplitude (see Supplemental Data). Upper panel: Typical 30 s intensity traces for a measurement of glycine buffer before (red) and after (black) the addition of 200 μl of SVs. The first 30 s after addition of SVs to the dye-containing buffer was analyzed in 5 s bins. Lower panel: Three typical autocorrelation functions were taken from such 5 s detection periods, which yielded the following numbers of particles per effective detection volume (0.14 fl in this particular example): ○ = 0.074, □ = 0.056, △ = 0.062 (black lines). The red trace is the ACF of a 5 s measurement of background fluorescence before addition of the vesicles.

(C) SV concentration determined by FCS plotted versus the protein concentration measured for the same sample, allowing the amount of protein per vesicle to be deduced for each test sample. The values from ten independent vesicle samples show a good correlation (means ± SEMs).

were only able to quantify the V1-B subunit. Part of the V1 subunit is known to dissociate during membrane purification (Moriyama and Nelson, 1989). We attempted to correct for this loss by comparing the relative enrichment of the V1-B subunit with that of the Vo-a subunit between the homogenate and an enriched vesicle fraction (Figure S6). The enrichment of the V1-B subunit in SVs was comparable to that of the Vo-a subunit, suggesting that dissociation was not a major factor. Thus, we conclude that the average copy number of the V-ATPase is close to 1 and certainly below 2.

In addition, we estimated for the copy number of 11 additional proteins (see legend of Figure 4; see also Table S2). These estimates are partly based on previous publications and partly based on rough values obtained from a combination of subcellular fractionation and comparison with recombinant standard proteins. While the numbers need to be refined in the future, they are used here as the "best guess" figures for the construction of the model. Individually, none of these proteins makes a major contribution to the overall structure of the vesicle, so errors of even a factor of two to three in a single case do not affect our conclusions. The sum of all proteins included in the model yields a mass of 11.5×10^{-18} g, i.e., ~67.5% of the estimated total mass contribution of all proteins in the vesicle.

The number of all phospholipid and cholesterol molecules per vesicle was calculated to be approximately 7000 and 5600, respectively, with hexosylceramides and gangliosides making only a relatively minor contribution (Table 2). Considering that a single phospholipid molecule occupies a space of approximately 65 $Å^2$ (0.65 nm^2) (Nagle and Tristram-Nagle, 2000), 7000 phospholipids would build a planar bilayer of 4550 nm^2, i.e., 50% of the outer and inner surfaces of a vesicle possessing an outer diameter of 42 nm. Furthermore, the total number of transmembrane domains in our model is 448. If one assumes that this number covers ~3/4 of all transmembrane

Table 2. Physical Parameters and Composition of an Average Synaptic Vesicle

Physical Parameters	
Density (g/ml)	1.10
Outer diameter (nm)	41.6
Inner aqueous volume (l)	19.86×10^{-21}
Number of neurotransmitter molecules (at 150 mM)	1790
Mass (g)[a]	29.6×10^{-18}
Mass (MDa)[a]	17.8
Protein:phospholipids (w:w)	1.94
Phospholipids:cholesterol (mol:mol)	1:0.8
Transmembrane domains (number/% of surface coverage)[b]	600/20.0
Protein Stoichiometry (Copies/Vesicle)	
Synaptophysin	31.5
Synaptobrevin/VAMP2	69.8
VGLUT1[c]	9.0
VGLUT2[c]	14.4
Synapsins	8.3
Syntaxin 1	6.2
SNAP-25	1.8
Synaptotagmin	15.2
Rab3A	10.3
SV2	1.7
Synaptogyrin	2.0
SCAMP1	0.8
CSP	2.8
V-ATPase[d]	1.4
NSF (hexamer)	0.2
Membrane Lipids	
Phospholipids total (number/% of surface coverage)	6992/50.4
Phosphatidylcholine	2524
Phosphatidylethanolamine (C1-ester/C1-ether)	1621/1311
Phosphatidylserine	857
Phosphatidylinositol	132
Sphingomyelin	516
Cholesterol	5663
Hexosylceramide	108

Mean values are shown.

[a] Calculated indirectly using the vesicle number and the sum of protein and lipid masses. In agreement with this result, a mass of $(26.4 \pm 5.8) \times 10^{-18}$ g was measured directly with STEM, which corresponds to 15.9 ± 3.5 MDa.

domains, the final number amounts to approximately 600. Considering that a single α helix in a membrane occupies approximately 150 Å^2 (1.5 nm^2, as estimated from the three-dimensional structures of the helical membrane proteins aquaporin-1 and the ClC chloride channel), the space requirement of all 600 transmembrane domains (if densely packed and oriented perpendicular to the membrane) amounts to 900 nm^2, i.e., 18% of the outer and 25% of the inner membrane surface. Thus, phospholipids plus transmembrane domains are calculated to cover about 70% of the vesicle surface. With the contribution of cholesterol to the surface area being unknown, the final estimate is reasonably close to that predicted on theoretical grounds, providing yet another criterion for the accuracy of the final model.

To visualize the SV structure, we constructed a correctly scaled model that attempts to attain atomic resolution wherever possible. Packing of a patch of membrane lipids was simulated by molecular dynamics, followed by vesicle construction using professional 3D software (see Experimental Procedures). The protein structures were modeled based on existing partial or complete crystal structures, structures of similar or homologous proteins, or secondary-structure predictions followed by short molecular dynamics simulations (see Experimental Procedures and Supplemental Data for details). Views of the resulting molecular model are shown in Figure 4; the individual proteins are color coded and labeled.

The final model is striking in that it shows how strongly trafficking organelles are dominated by their protein constituents. To confirm that the surface of a SV is covered by protein, we used three different electron microscopic procedures, all suitable for imaging surface proteins. The procedures include cryoelectron microscopy (shock-frozen samples, no heavy-metal contrasting); platinum shadowing of mica-adsorbed, freeze-dried specimens; and dark-field STEM of negatively stained vesicles. Figure 5 shows galleries of vesicle images obtained by each of the methods. There is considerable variability in surface and membrane structure. All three methods show the surface to be covered with amorphous structures and, in some cases, large globular structures. These structures represent proteins because they were removed by a pronase digestion (Figure 5D). Figure 5E shows the reconstruction of one of the large surface blobs based on a tilt series obtained in the cryoelectron microscope. It exhibits features of the V-ATPase (Wilkens et al., 2005), a globular head being connected to the vesicle surface via a stalk. The number of these large structures per vesicles was variable, with most vesicles containing one or two, in

[b] Estimate; the number calculated from the proteins included in the model (Figure 4) amounts to 497 (see Table S2 for details).

[c] Corrected for the fraction of vesicles found to be positive by immunogold electron microscopy for the respective transporter.

[d] Adjusted to compensate for the loss of the V1 subunit (see text).

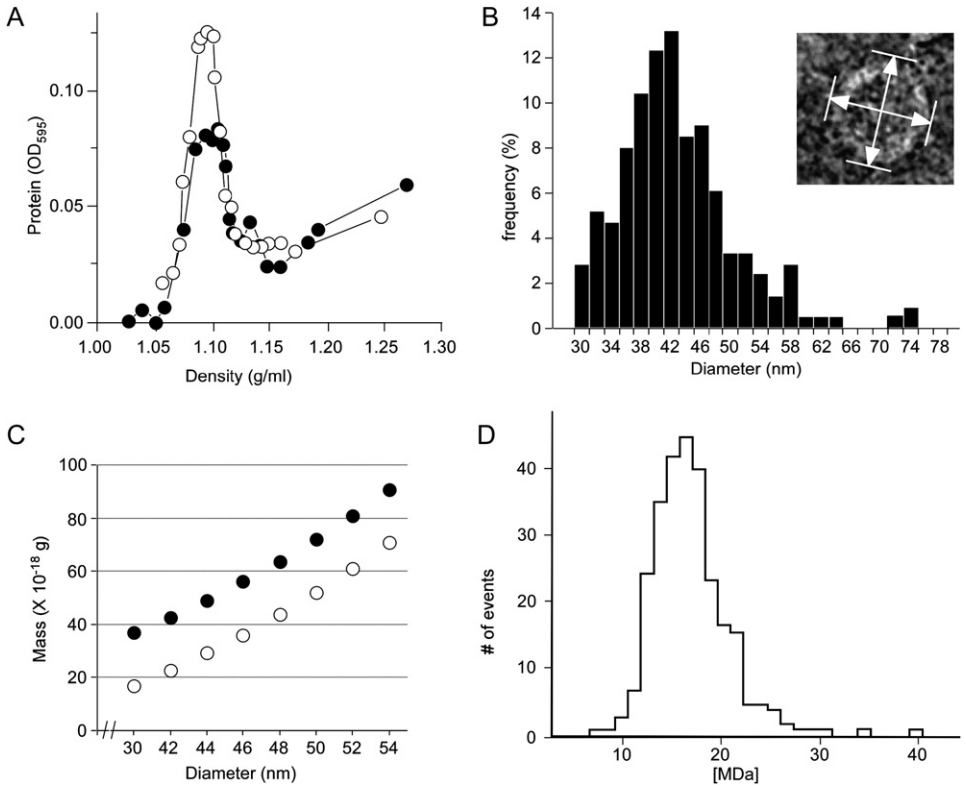

Figure 3. Physical Characterization of SVs

(A) Determination of the buoyant density of SVs using iodixanol density gradients. Purified SVs were either loaded on the top of the iodixanol gradient (○) (5%–35%, which corresponds to a density range of 1.04–1.22 g/ml) or added to each gradient solution at equal concentration (●) (for details, see Supplemental Data). After centrifugation for 5 hr at 180,000 × g, fractions of 500 μl were collected. Protein concentrations (determined according to Bradford, 1976) were plotted against density, which was calculated from the refractive index. The vesicle distribution shows a peak at a density of 1.10 g/ml, regardless of whether the sample was loaded on top of the gradient (○) or mixed with the gradient solution (●).

(B) Size distribution of SVs, determined by cryoelectron microscopy (n = 790). Diameters were measured from the outer rims of the bilayer. To account for size irregularities, two measurements orthogonal to each other were taken and averaged (see inset).

(C) Mass/diameter relationship calculated using a particle density (ρ) of 1.10 g/ml. Assuming that the vesicles are perfectly spherical, the mass (m) can be calculated according to $m = (4\pi r^3/3)\rho$, where r is the radius and ρ is the density of the particle. ● indicates the total mass of the particle. To estimate the dry mass (○), vesicles were assumed to be filled with isolation buffer (density approximately 1.0 g/ml) and to have a volume corresponding to the inner volume of the vesicle (diameter corrected for a membrane thickness of 4.0 nm).

(D) Mass distribution of SVs determined by scanning transmission electron microscopy (STEM). The histogram displays the mass of 281 vesicles from both untreated and glutaraldehyde-stabilized samples (see Figure S5). The average value is 16.2 ± 4.1 MDa ([26.9 ± 6.8] × 10^{-18} g/vesicle; n = 281) or 15.9 ± 3.5 MDa ([26.4 ± 5.8] × 10^{-18} g/vesicle, n = 276), excluding the few very high values, and the main peak is at 15.4 ± 3.1 MDa ([25.6 ± 5.1] × 10^{-18} g/vesicle).

agreement with previous observations (Stadler and Tsukita, 1984).

DISCUSSION

In the present study, we have used an array of modern molecular, biophysical, electron microscopy, and modeling techniques to arrive at a quantitative description of a SV, as a model trafficking organelle. A 3D model was constructed in which it was attempted to achieve atomic resolution wherever possible (Figure 4). The results provide a benchmark for future studies of trafficking organelles and yield insights into the molecular constraints that govern the various functions a SV must perform, while shedding new light on the structure of a typical membrane functioning in the secretory pathway of eukaryotic cells.

SV Proteome and Compositional Heterogeneity

SVs are the best characterized of all organelles. Many membrane proteins have been described previously (Jahn and Südhof, 1994; Lin and Scheller, 2000), most of which were found in our proteome analysis. Only a few novel putative membrane proteins were identified, and it remains to be established whether these were contaminants or genuine vesicle residents. Although we cannot exclude the presence of additional unknown

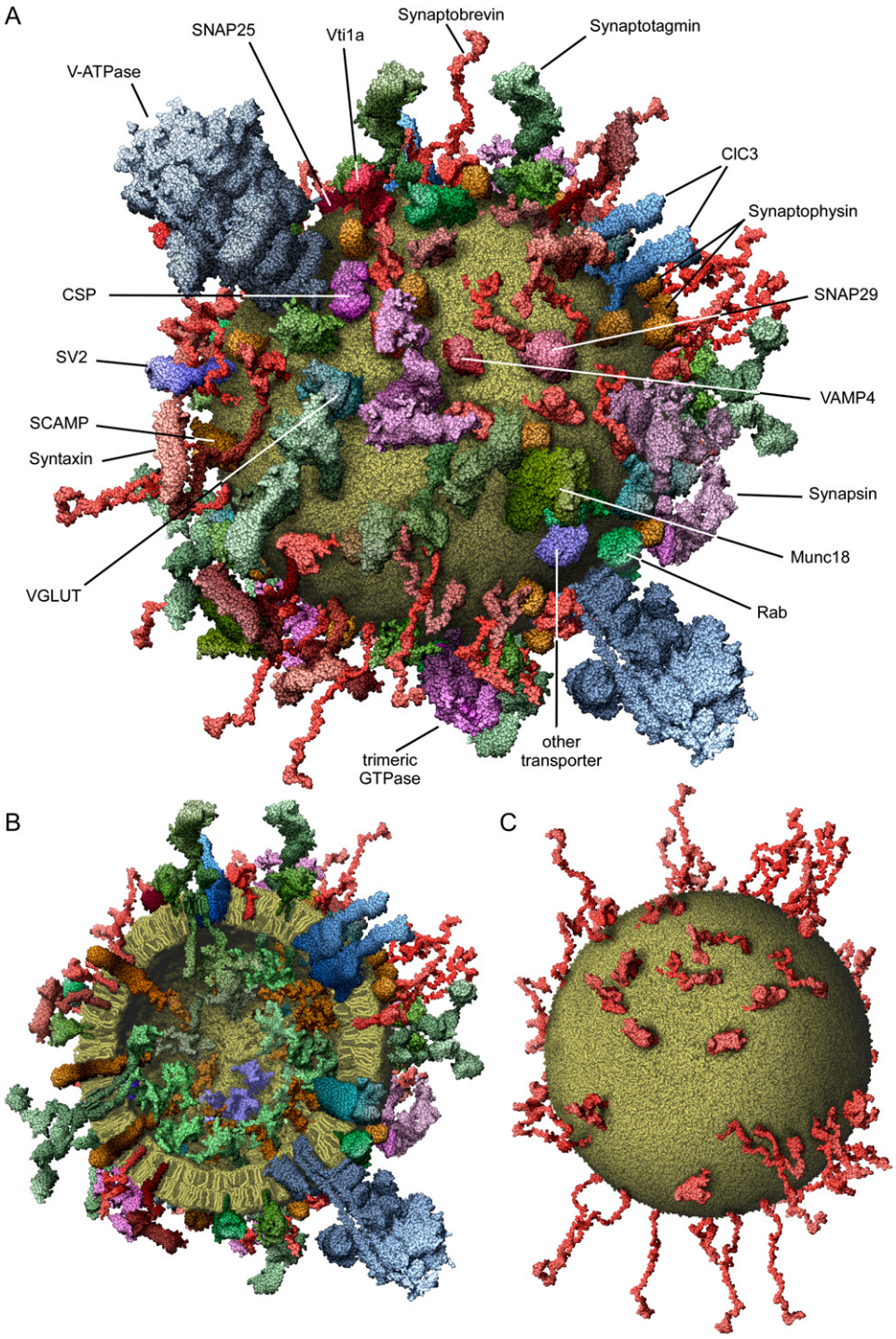

Figure 4. Molecular Model of an Average SV

The model is based on space-filling models of all macromolecules at near atomic resolution.

(A) Outside view of a vesicle.

(B) View of a vesicle sectioned in the middle (the dark-colored membrane components represent cholesterol).

(C) Model containing only synaptobrevin to show the surface density of the most abundant vesicle component.

In addition to the proteins listed in Table 2, the following proteins were included (copy number in parentheses): VAMP4 (2), SNAP-29 (1), vti1a (2) syntaxin 6 (2), other syntaxins (4), other synaptotagmins (5), other Rab proteins (15), Munc-18 (2), other transporters (2), chloride channels (2), and trimeric GTPases (2) (see Table S2 for more details).

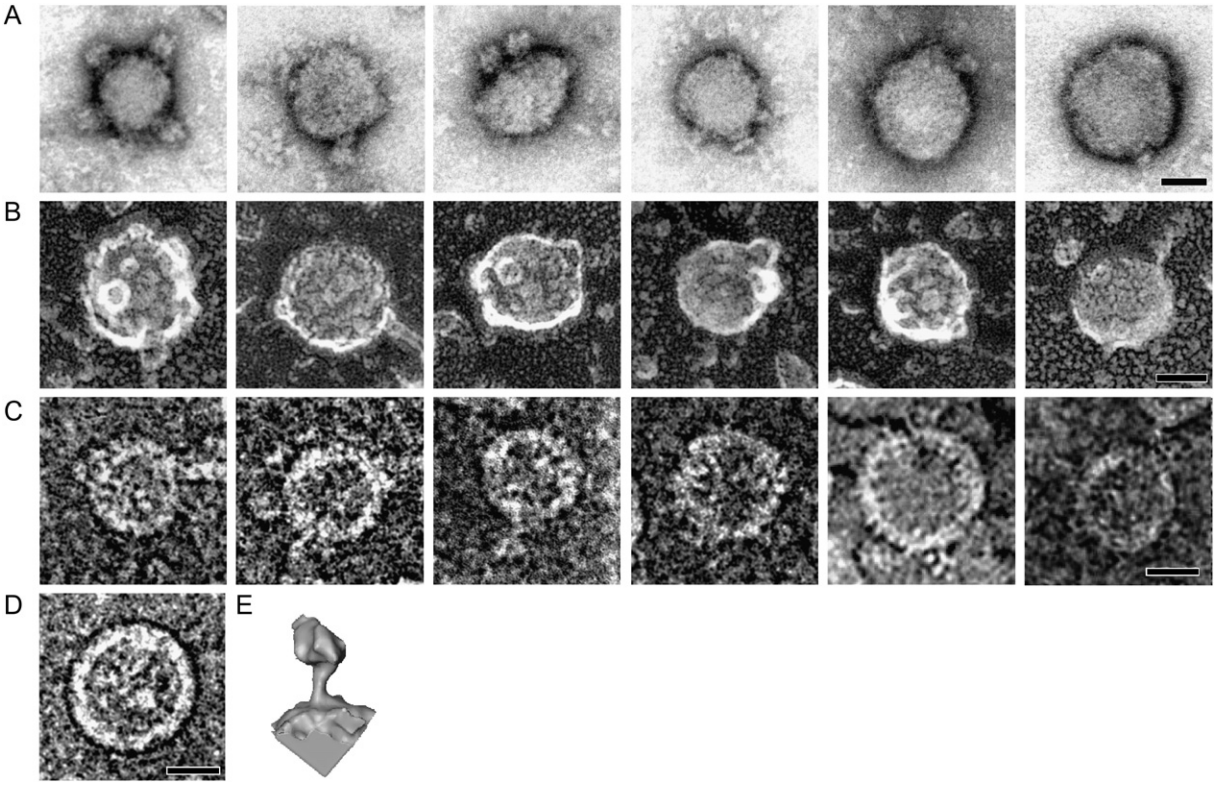

Figure 5. Synaptic Vesicles Imaged by Independent Electron Microscopy Procedures

(A) Negatively stained by uranyl acetate and imaged by STEM. Scale bar in (A)–(D) = 20 nm.

(B) Platinum shadowed after quick-freeze/deep etching.

(C) Native cryopreparation.

(D) As in (C), but after digestion by pronase treatment of surface proteins (100 μg SVs were digested with 100 μg pronase for 2 hr at 30°C). Note that the bilayer is more clearly visible after protease treatment.

(E) Electron tomographic model of a single large structural element located at the vesicle surface (presumably a V-ATPase).

proteins, we regard this as rather unlikely considering the high coverage of known proteins in our proteome analysis.

The proteomes of both SVs (Morciano et al., 2005) and brain-derived clathrin-coated vesicles (Blondeau et al., 2004) have recently been investigated by other laboratories. In the former study, approximately 80 different proteins were identified, most of which were detected and included in our analysis. Considering how difficult it is to prepare subcellular fractions free of contamination, this is an excellent agreement, particularly as Morciano et al. (2005) used a different vesicle isolation protocol (separation on density gradients followed by immunoisolation using SV2 antibodies). In the clathrin-coated vesicle fraction, approximately 200 proteins were identified, including many of the major SV proteins. About 30 proteins were tested for comigration with clathrin-coated vesicles during gradient centrifugation. In both earlier studies, the recovery of known vesicle membrane proteins was lower than in our analysis (which is also incomplete), highlighting the need for improvements in the proteomic analysis of membrane proteins.

To what extent are SVs isolated from brain heterogeneous in their protein composition? Analysis of glutamatergic and GABAergic vesicle subpopulations revealed no difference with respect to more than a dozen major vesicle proteins (Takamori et al., 2000a, 2000b). Furthermore, while most SV proteins such as synapsins, synaptobrevins, synaptotagmins, synaptophysins, SV2s, and SCAMPs occur in several isoforms displaying differential localization in the CNS, it appears that each synapse and each vesicle contain at least one of the isoforms of each family (Jahn and Südhof, 1994). Although we cannot exclude that the copy number of individual vesicle proteins may vary between different neurons, or even between individual vesicles, we conclude that SVs share a basic set of common proteins, to which the model shown in Figure 4 is confined.

As well as the common set of "genuine" vesicle residents, the SV proteome contains many proteins that are probably "visitors" only associating with a SV for part of its life cycle. Several of these proteins are large, such as CaM kinase II, chaperones, and the AAA+ ATPase NSF. It is likely that the structural heterogeneity documented

in Figure 5 is largely due to heterogeneous occupancy by such accessory proteins.

Implications for Membrane Structure

Generally, the physical features of biological membranes are thought to be dominated by the lipid bilayer, in which integral membrane proteins are embedded as independent and diffusible entities (Singer and Nicolson, 1972). Our data now show that the SV membrane has a higher protein density than anticipated, with a quarter of the entire membrane volume being taken up by transmembrane domains (130×10^3 transmembrane regions/μm^2; for reference, in paracrystalline arrays of acetylcholine receptors, the receptor density is approximately 20,000/μm^2, amounting to 400×10^3 transmembrane regions/μm^2 [Brisson and Unwin, 1984]). If a monomolecular "collar" of bound phospholipids surrounded each membrane protein, the majority of phospholipid molecules would not be free. We do not know whether the membrane proteins are separate entities or form clusters within the vesicle membrane, although there is some support for the latter possibility (Bennett et al., 1992). The high density of transmembrane domains is expected to put constraints on the mobility of the membrane lipids that may be required for optimal packing of the crowded proteins. A picture is emerging in which the membrane resembles a cobblestone pavement, with the proteins organized in patches that are surrounded by lipidic rims, rather than icebergs floating in a sea of lipids. This is compatible with recent measurements of the diffusional behavior of membrane proteins (Ritchie et al., 2005). Note that the model shown in Figure 4 only accounts for approximately 2/3 of the protein mass of SVs. It can be envisioned that, viewed from the outside, the lipidic surface is hardly "visible" when all proteins are present, which is supported by the EM images of vesicles obtained by platinum shadowing (Figure 5). Nevertheless, we cannot exclude the possibility that a significant portion of the membrane proteins are organized in large clusters, leaving patches of lipids that do not interact with proteins and are freely diffusible.

Implications for Membrane Trafficking

One of the unexpected outcomes of our quantitative analysis is the high surface density of the R-SNARE synaptobrevin, which outnumbers synaptophysin and synaptotagmin by a factor of three or more (Table 2). Since the fully assembled core complex has a length of 12 nm, a separation of less than 20 nm is probably required for the initiation of SNARE *trans*-complexes. Assuming that synaptobrevin is distributed equally across the vesicle surface (Figure 4C), 12 synaptobrevin molecules would be in this range when the membranes are still separated by a distance of 5 nm. Thus, the surface density of synaptobrevin does not appear to be rate limiting. From our data, it would seem that only a fraction of the synaptobrevin molecules are engaged in SNARE complex formation during each fusion event, so it is conceivable that vesicles may fuse repetitively even if disassembly of SNARE complexes is slowed down or inactivated. This is in agreement with previous findings on a temperature-sensitive NSF mutant (comatose) in *Drosophila* (Littleton et al., 1998). Similarly, the copy number of synaptotagmin and Rab proteins is high. Apparently, these essential trafficking proteins have a comfortable "safety margin" ensuring that sufficient copies of each protein are "on board" during repetitive rounds of recycling.

Implications for Neurotransmitter Uptake and Storage

SVs contain neurotransmitter transporters that are fueled by a proton electrochemical gradient (reviewed in Ahnert-Hilger et al., 2003). Our results show that vesicles contain approximately ten copies of either VGLUT1 or VGLUT2, and it is likely that the copy number for VGAT, VAChT, or VMAT1/2 is similar on the respective vesicles. With a membrane thickness of 4 nm, the inner volume of an average vesicle is 19.86×10^{-21} l, equal to 1790 molecules of glutamate assuming a concentration of 150 mM (Table 2). The transport rates of the vesicular carriers are not known. However, even if they translocate only ten molecules/s (which would render these transporters among the slowest known carriers; Peters, 2003), refilling of an empty vesicle is possible within 20 s, which is more than enough to completely fill a vesicle under conditions of high activity and short recycling times. Indeed, it has recently been shown that a single transporter molecule may suffice to fill a SV (Daniels et al., 2006). It needs to be remembered, however, that the neurotransmitter content appears to be determined, at least to some extent, by the copy number of transporters, suggesting that there is an equilibrium between uptake and efflux (Williams, 1997; Pothos et al., 2000; Wojcik et al., 2004).

Surprisingly, vesicles contain less than two copies of the vacuolar ATPase, making it the sole exception among proteins known to be essential for vesicle function. While a single copy may be sufficient to fit the energetic needs of neurotransmitter uptake, a high fidelity of trafficking is needed to ensure that a SV contains one copy of this essential enzyme during each round of recycling. However, it is also possible that a vesicle may fail to incorporate a V-ATPase during formation. Such a vesicle would remain empty and thus "silent," but it would still be capable of undergoing fusion and recycling, thus getting another chance to incorporate a copy of the V-ATPase.

It has previously been suggested that SVs contain a macromolecular matrix that may serve as a "smart polymer," allowing neurotransmitter to be stored in an osmotically inactive form (see, e.g., Reigada et al., 2003). EM tomography of neuromuscular endplates suggested the presence of macromolecular material within the lumen of cholinergic vesicles while the vesicle surface was surprisingly smooth (Harlow et al., 2001). Presently, we cannot exclude the existence of such macromolecular material, at least not in a small vesicle subpopulation as represented by cholinergic and aminergic vesicles. However, in all our biochemical and biophysical experiments thus

far, we have been unable to detect any evidence for such a polymer.

Conclusion

In recent years, we have witnessed major advances concerning the molecular mechanisms underlying membrane trafficking. However, quantitative information about the proteins or protein complexes involved is still scarce. Furthermore, the overall structure of a trafficking organelle as an entity has not been described in a quantitative manner. The work presented here will hopefully contribute to closing this gap and provide a useful point of departure for quantitative work on trafficking, docking, and fusion and for the development of molecular models.

EXPERIMENTAL PROCEDURES

Purification of SVs from Rat Brain

SVs were purified from rat brain, as described in detail in previous publications (Nagy et al., 1976; Huttner et al., 1983) (see also Figure S1). To remove peripheral proteins from the SVs, the purified vesicle fraction was resuspended with a 28-gauge needle in 0.1 M Na_2CO_3 (pH 11) and incubated on ice for 15 min. Immediately afterwards, the vesicles were collected by centrifugation at 50,000 rpm for 20 min in a Beckman Ti 100.2 rotor.

Protein and Lipid Analysis

Vesicle proteins were separated either by 1D SDS-PAGE (Laemmli, 1970) or 2D electrophoresis using the 16-BAC/SDS-PAGE system (Hartinger et al., 1996). After Coomassie blue staining, all visible spots were excised, cut into ~1 mm^2 pieces, and subjected to in-gel trypsinization (Shevchenko et al., 1996). The extracted peptides were analyzed by liquid chromatography-tandem mass spectrometry (LC-MS/MS) on a Q-TOF Ultima mass spectrometer (Waters), and proteins were identified in the NCBI nonredundant database using Mascot (Matrix Science, London) as a search engine. To determine the false-discovery rate (Elias et al., 2005), the data (PKL files) were searched against a randomized NCBInr database.

Purified standard proteins were prepared for the quantification of individual proteins on SVs. Synaptobrevin, syntaxin, and SNAP-25 (Schuette et al., 2004) and the V1-B subunit of the rat V-ATPase were prepared as full-length recombinant proteins. Native synaptophysin was affinity purified from rat brain (Navone et al., 1986), as were VGLUT1 and VGLUT2 (Takamori et al., 2001).

For syntaxin 1, SNAP-25, synaptophysin, VGLUT1, VGLUT2, and the V1-B subunit of the V-ATPase, a preparative gel electrophoresis was performed as a final purification step, followed by electroelution. Where unmodified full-length protein standards were available, quantitative western blots were performed. For all other proteins, we performed a dot-blot analysis (Jahn et al., 1984). In both cases, immunoreactivities were detected by using ^{125}I-conjugated protein A and the images were acquired with a Fuji BAS-2500 reader. Signal intensities were evaluated using Raytest AIDA image analysis software.

Lipid extraction, nano-ESI-MS/MS, and quantitative analyses were performed as described (Brügger et al., 1997, 2000) (see also Supplemental Data).

Electron Microscopy

For cryoelectron microscopy, a solution containing purified SVs was applied to perforated carbon-coated grids and rapidly frozen in liquid ethane. Images were taken on negative film at a magnification of 50,000× and a defocus of −2.3 mm using a Gatan cryostage in a Philips CM120 electron microscope. Micrographs were digitized using a flat-bed scanner (Duoscan T2500, Agfa-Gevaert) with a resolution of 1200 dpi. The longest and shortest diameters (outer rim) of each vesicle were measured with Digital Migrograph 3.4 software (Gatan) (Schuette et al., 2004) and averaged to produce the mean vesicle diameter.

For the negative-stain microscopy, a solution containing SVs was applied to a glow-discharged carbon-coated grid, washed with 100 mM ammonium acetate, and stained with 2% uranyl acetate. Digital dark-field images were recorded using a Vacuum Generators STEM HB-5 microscope at an accelerating voltage of 100 kV and a magnification of 560,000× (recording dose, 7000 electrons/nm^2). The contrast of the images shown has been adjusted to display protein in bright shades.

For preparation of platinum replicas, purified vesicles were adsorbed to a suspension of finely ground mica flakes, followed by freeze drying and platinum replication according to established procedures (Heuser, 1989).

Scanning transmission electron microscopy was employed to determine the vesicle mass, essentially using procedures described previously (Müller et al., 1992); see Supplemental Data for details.

Molecular Dynamics Simulations and Model Construction

To simulate the lipid membrane, a patch consisting of 128 dimyristoylphosphatidylcholine (DMPC) and 64 cholesterol molecules solvated in 3655 SPC (Berendsen et al., 1981) water molecules was constructed. This patch was equilibrated in a periodic simulation box for 12 nanoseconds using molecular dynamics (for details, see Supplemental Data). A vesicle was constructed from this equilibrated patch as follows. The patch was transferred to the 3D program Maya (Autodesk). To obtain a more natural patch, the orientation (and partially, the position and tilt of the lipids) was adjusted to meet the curvature of a SV. This new patch was then duplicated and further manipulated (more lipids were added to fill the evolving gaps) to obtain complete coverage of the entire vesicle.

Domains or whole proteins for which no high-resolution structure was available were completely constructed in the 3D program using information from secondary-structure prediction programs with respect to α helices and β sheets. Predicted "random coils" were modeled in a compact manner before being converted into PDB files and refined by short molecular dynamics simulations. Known partial structures of proteins were completed by attaching modeled domains. Where available, the structures of homologous proteins were used to build the corresponding protein (homology modeling). A set of final structures was obtained from different snapshots of the molecular dynamics trajectories. A list of all high-resolution structures used for modeling is provided in the Supplemental Data.

Miscellaneous Procedures

Protein concentration was determined by a modified Lowry assay (Peterson, 1977). For some reference proteins whose yields were limited (such as VGLUT1 and VGLUT2, which were immunoaffinity purified from rat brains), the BCA Assay Kit from Pierce with the enhanced protocol was used. The antibodies used in this study are listed in Supplemental Data.

Supplemental Data

Supplemental Data include Supplemental Experimental Procedures, Supplemental References, six figures, and two tables and can be found with this article online at http://www.cell.com/cgi/content/full/127/4/831/DC1/.

ACKNOWLEDGMENTS

The authors are indebted to the following for reagents, help, and/or advice: A. Stein, M. Druminski, S.O. Rizzoli, and M. Raabe (Göttingen, Germany); A. Engel, R. Buerki, and F. Erne-Brand (Basel, Switzerland); V. Krzyzanek (Münster, Germany); and K.M. Harris (Augusta, GA, USA). We apologize to all colleagues whose work, although relevant,

could not be quoted due to space limitations. S.T. was supported by JSPS in part during this work. M.G. was supported by the Danish Agency for Science, Technology and Innovation (DASTI). S.A.M. was supported by the Maurice E. Müller Foundation of Switzerland and the Swiss National Foundation (grant number 3100-059415). R.J. acknowledges generous support from the Gottfried-Wilhelm Leibniz Program of the DFG and Fonds der Chemischen Industrie.

This article is dedicated to Victor P. Whittaker (Cambridge University) in honor of his pioneering work on synaptic vesicles.

Received: May 5, 2006
Revised: July 27, 2006
Accepted: October 12, 2006
Published: November 16, 2006

REFERENCES

Ahnert-Hilger, G., Höltje, M., Pahner, I., Winter, S., and Brunk, I. (2003). Regulation of vesicular neurotransmitter transporters. Rev. Physiol. Biochem. Pharmacol. *150*, 140–160.

Antonin, W., Riedel, D., and Fischer von Mollard, G. (2000). The SNARE Vti1a-beta is localized to small synaptic vesicles and participates in a novel SNARE complex. J. Neurosci. *20*, 5724–5732.

Benfenati, F., Greengard, P., Brunner, J., and Bähler, M. (1989). Electrostatic and hydrophobic interactions of synapsin I and synapsin I fragments with phospholipid bilayers. J. Cell Biol. *108*, 1851–1862.

Bennett, M.K., Calakos, N., Kreiner, T., and Scheller, R.H. (1992). Synaptic vesicle membrane proteins interact to form a multimeric complex. J. Cell Biol. *116*, 761–775.

Berendsen, H.J.C., Postma, J.P.M., van Gunsteren, W.F., and Hermans, J. (1981). Interaction models for water in relation to protein hydration. In Intermolecular Forces, B. Pullman, ed. (Dordrecht, The Netherlands: D. Riedel Publishing Company), pp. 331–342.

Blondeau, F., Ritter, B., Allaire, P.D., Wasiak, S., Girard, M., Hussain, N.K., Angers, A., Legendre-Guillemin, V., Roy, L., Boismenu, D., et al. (2004). Tandem MS analysis of brain clathrin-coated vesicles reveals their critical involvement in synaptic vesicle recycling. Proc. Natl. Acad. Sci. USA *101*, 3833–3838.

Bock, J.B., Matern, H.T., Peden, A.A., and Scheller, R.H. (2001). A genomic perspective on membrane compartment organization. Nature *409*, 839–841.

Bonifacino, J.S., and Glick, B.S. (2004). The mechanisms of vesicle budding and fusion. Cell *116*, 153–166.

Bradford, M.M. (1976). A rapid and sensitve method for the quantitation of microgram quantities of protein utilizing the principle of protein-dye binding. Anal. Biochem. *72*, 248–254.

Brisson, A., and Unwin, P.N. (1984). Tubular crystals of acetylcholine receptor. J. Cell Biol. *99*, 1202–1211.

Brügger, B., Erben, G., Sandhoff, R., Wieland, F.T., and Lehmann, W.D. (1997). Quantitative analysis of biological membrane lipids at the low picomole level by nano electrospray ionization tandem mass spectrometry. Proc. Natl. Acad. Sci. USA *94*, 2339–2344.

Brügger, B., Sandhoff, R., Wegehingel, S., Gorgas, K., Malsam, J., Helms, J.B., Lehmann, W.D., Nickel, W., and Wieland, F.T. (2000). Evidence for segregation of sphingomyelin and cholesterol during formation of COPI-coated vesicles. J. Cell Biol. *151*, 507–518.

Chapman, E.R., and Jahn, R. (1994). Calcium-dependent interaction of the cytoplasmic region of synaptotagmin with membranes. Autonomous function of a single C2-homologous domain. J. Biol. Chem. *269*, 5735–5741.

Daniels, R.W., Collins, C.A., Chen, K., Gelfand, M.V., Featherstone, D.E., and DiAntonio, A. (2006). A single vesicular glutamate transporter is sufficient to fill a synaptic vesicle. Neuron *49*, 11–16.

de Hoop, M.J., Huber, L.A., Stenmark, H., Williamson, E., Zerial, M., Parton, R.G., and Dotti, C.G. (1994). The involvement of the small GTP-binding protein Rab5a in neuronal endocytosis. Neuron *13*, 11–22.

Elias, J.E., Haas, W., Faherty, B.K., and Gygi, S.P. (2005). Comparative evaluation of mass spectrometry platforms used in large-scale proteomics investigations. Nat. Methods *2*, 667–675.

Engel, A. (1978). Molecular weight determination by scanning transmission electron microscopy. Ultramicroscopy *3*, 273–281.

Fischer von Mollard, G., Stahl, B., Khokhlatchev, A., Südhof, T.C., and Jahn, R. (1994a). Rab3C is a synaptic vesicle protein that dissociates from synaptic vesicles after stimulation of exocytosis. J. Biol. Chem. *269*, 10971–10974.

Fischer von Mollard, G., Stahl, B., Walch-Solimena, C., Takei, K., Daniels, L., Khoklatchev, A., De Camilli, P., Südhof, T.C., and Jahn, R. (1994b). Localization of Rab5 to synaptic vesicles identifies endosomal intermediate in synaptic vesicle recycling pathway. Eur. J. Cell Biol. *65*, 319–326.

Fremeau, R.T., Jr., Troyer, M.D., Pahner, I., Nygaard, G.O., Tran, C.H., Reimer, R.J., Bellocchio, E.E., Fortin, D., Storm-Mathisen, J., and Edwards, R.H. (2001). The expression of vesicular glutamate transporters defines two classes of excitatory synapse. Neuron *31*, 247–260.

Goelz, S.E., Nestler, E.J., Chehrazi, B., and Greengard, P. (1981). Distribution of protein I in mammalian brain as determined by a detergent-based radioimmunoassay. Proc. Natl. Acad. Sci. USA *78*, 2130–2134.

Harlow, M.L., Ress, D., Stoschek, A., Marshall, R.M., and McMahan, U.J. (2001). The architecture of active zone material at the frog's neuromuscular junction. Nature *409*, 479–484.

Harris, K.M., and Sultan, P. (1995). Variation in the number, location and size of synaptic vesicles provides an anatomical basis for the nonuniform probability of release at hippocampal CA1 synapses. Neuropharmacology *34*, 1387–1395.

Hartinger, J., Stenius, K., Hogemann, D., and Jahn, R. (1996). 16-BAC/SDS-PAGE: A two-dimensional gel electrophoresis system suitable for the separation of integral membrane proteins. Anal. Biochem. *240*, 126–133.

Heuser, J. (1989). Protocol for 3-D visualization of molecules on mica via the quick-freeze, deep-etch technique. J. Electron Microsc. Tech. *13*, 244–263.

Holt, M., Varoqueaux, F., Wiederhold, K., Takamori, S., Urlaub, H., Fasshauer, D., and Jahn, R. (2006). Identification of SNAP-47, a novel Qbc-snare with ubiquitous expression. J. Biol. Chem. *281*, 17076–17083.

Huttner, W.B., Schiebler, W., Greengard, P., and De Camilli, P. (1983). Synapsin I (protein I), a nerve terminal-specific phosphoprotein. III. Its association with synaptic vesicles studied in a highly purified synaptic vesicle preparation. J. Cell Biol. *96*, 1374–1388.

Jahn, R., and Südhof, T.C. (1994). Synaptic vesicles and exocytosis. Annu. Rev. Neurosci. *17*, 219–246.

Jahn, R., Schiebler, W., and Greengard, P. (1984). A quantitative dot-immunobinding assay for proteins using nitrocellulose membrane filters. Proc. Natl. Acad. Sci. USA *81*, 1684–1687.

Janz, R., Hofmann, K., and Sudhof, T.C. (1998). SVOP, an evolutionarily conserved synaptic vesicle protein, suggests novel transport functions of synaptic vesicles. J. Neurosci. *18*, 9269–9281.

Khvotchev, M.V., Ren, M., Takamori, S., Jahn, R., and Südhof, T.C. (2003). Divergent functions of neuronal Rab11b in Ca^{2+}-regulated versus constitutive exocytosis. J. Neurosci. *23*, 10531–10539.

Laemmli, U.K. (1970). Cleavage of structural proteins during the assembly of the head of bacteriophage T4. Nature *227*, 680–685.

Lin, R.C., and Scheller, R.H. (2000). Mechanisms of synaptic vesicle exocytosis. Annu. Rev. Cell Dev. Biol. *16*, 19–49.

Littleton, J.T., Chapman, E.R., Kreber, R., Garment, M.B., Carlson, S.D., and Ganetzky, B. (1998). Temperature-sensitive paralytic mutations demonstrate that synaptic exocytosis requires SNARE complex assembly and disassembly. Neuron *21*, 401–413.

Magde, D., Elson, E., and Webb, W.W. (1972). Thermodynamic fluctuations in a reacting System - Measurement by Fluorescence Correlation Spectroscopy. Phys. Rev. Lett. *29*, 705–708.

Maycox, P.R., Link, E., Reetz, A., Morris, S.A., and Jahn, R. (1992). Clathrin-coated vesicles in nervous tissue are involved primarily in synaptic vesicle recycling. J. Cell Biol. *118*, 1379–1388.

Morciano, M., Burre, J., Corvey, C., Karas, M., Zimmermann, H., and Volknandt, W. (2005). Immunoisolation of two synaptic vesicle pools from synaptosomes: a proteomics analysis. J. Neurochem. *95*, 1732–1745.

Moriyama, Y., and Nelson, N. (1989). Cold inactivation of vacuolar proton-ATPases. J. Biol. Chem. *264*, 3577–3582.

Muller, J.D., Chen, Y., and Gratton, E. (2003). Fluorescence correlation spectroscopy. Methods Enzymol. *361*, 69–92.

Müller, S.A., Goldie, K.N., Bürki, R., Häring, R., and Engel, A. (1992). Factors influencing the precision of quantitative scanning transmission electron microscopy. Ultramicroscopy *46*, 317–334.

Nagle, J.F., and Tristram-Nagle, S. (2000). Structure of lipid bilayers. Biochim. Biophys. Acta *1469*, 159–195.

Nagy, A., Baker, R.R., Morris, S.J., and Whittaker, V.P. (1976). The preparation and characterization of synaptic vesicles of high purity. Brain Res. *109*, 285–309.

Navone, F., Jahn, R., Di Gioia, G., Stukenbrok, H., Greengard, P., and De Camilli, P. (1986). Protein p38: an integral membrane protein specific for small vesicles of neurons and neuroendocrine cells. J. Cell Biol. *103*, 2511–2527.

Peters, R. (2003). Optical single transporter recording: transport kinetics in microarrays of membrane patches. Annu. Rev. Biophys. Biomol. Struct. *32*, 47–67.

Peterson, G.L. (1977). A simplification of the protein assay method of Lowry et al. which is more generally applicable. Anal. Biochem. *83*, 346–356.

Pfeffer, S., and Aivazian, D. (2004). Targeting Rab GTPases to distinct membrane compartments. Nat. Rev. Mol. Cell Biol. *5*, 886–896.

Pothos, E.N., Larsen, K.E., Krantz, D.E., Liu, Y., Haycock, J.W., Setlik, W., Gershon, M.D., Edwards, R.H., and Sulzer, D. (2000). Synaptic vesicle transporter expression regulates vesicle phenotype and quantal size. J. Neurosci. *20*, 7297–7306.

Reigada, D., Diez-Perez, I., Gorostiza, P., Verdaguer, A., Gomez de Aranda, I., Pineda, O., Vilarrasa, J., Marsal, J., Blasi, J., Aleu, J., and Solsona, C. (2003). Control of neurotransmitter release by an internal gel matrix in synaptic vesicles. Proc. Natl. Acad. Sci. USA *100*, 3485–3490.

Ritchie, K., Shan, X.Y., Kondo, J., Iwasawa, K., Fujiwara, T., and Kusumi, A. (2005). Detection of non-brownian diffusion in the cell membrane in single molecule tracking. Biophys. J. *88*, 2266–2277.

Schlüter, O.M., Khvotchev, M., Jahn, R., and Südhof, T.C. (2002). Localization versus function of Rab3 proteins. Evidence for a common regulatory role in controlling fusion. J. Biol. Chem. *277*, 40919–40929.

Schuette, C.G., Hatsuzawa, K., Margittai, M., Stein, A., Riedel, D., Küster, P., König, M., Seidel, C., and Jahn, R. (2004). Determinants of liposome fusion mediated by synaptic SNARE proteins. Proc. Natl. Acad. Sci. USA *101*, 2858–2863.

Shevchenko, A., Wilm, M., Vorm, O., and Mann, M. (1996). Mass spectrometric sequencing of proteins silver-stained polyacrylamide gels. Anal. Chem. *68*, 850–858.

Singer, S.J., and Nicolson, G.L. (1972). The fluid mosaic model of the structure of cell membranes. Science *175*, 720–731.

Stadler, H., and Tsukita, S. (1984). Synaptic vesicles contain an ATP-dependent proton pump and show 'knob-like' protrusions on their surface. EMBO J. *3*, 3333–3337.

Stobrawa, S.M., Breiderhoff, T., Takamori, S., Engel, D., Schweizer, M., Zdebik, A.A., Bosl, M.R., Ruether, K., Jahn, H., Draguhn, A., et al. (2001). Disruption of ClC-3, a chloride channel expressed on synaptic vesicles, leads to a loss of the hippocampus. Neuron *29*, 185–196.

Südhof, T.C. (2004). The synaptic vesicle cycle. Annu. Rev. Neurosci. *27*, 509–547.

Takamori, S., Rhee, J.S., Rosenmund, C., and Jahn, R. (2000a). Identification of a vesicular glutamate transporter that defines a glutamatergic phenotype in neurons. Nature *407*, 189–194.

Takamori, S., Riedel, D., and Jahn, R. (2000b). Immunoisolation of GABA-specific synaptic vesicles defines a functionally distinct subset of synaptic vesicles. J. Neurosci. *20*, 4904–4911.

Takamori, S., Rhee, J.S., Rosenmund, C., and Jahn, R. (2001). Identification of differentiation-associated brain-specific phosphate transporter as a second vesicular glutamate transporter (VGLUT2). J. Neurosci. *21*, RC182.

Walch-Solimena, C., Blasi, J., Edelmann, L., Chapman, E.R., Fischer von Mollard, G., and Jahn, R. (1995). The t-SNAREs syntaxin 1 and SNAP-25 are present on organelles that participate in synaptic vesicle recycling. J. Cell Biol. *128*, 637–645.

Wilkens, S., Zhang, Z., and Zheng, Y. (2005). A structural model of the vacuolar ATPase from transmission electron microscopy. Micron *36*, 109–126.

Williams, J. (1997). How does a vesicle know it is full? Neuron *18*, 683–686.

Wojcik, S.M., Rhee, J.S., Herzog, E., Sigler, A., Jahn, R., Takamori, S., Brose, N., and Rosenmund, C. (2004). An essential role for vesicular glutamate transporter 1 (VGLUT1) in postnatal development and control of quantal size. Proc. Natl. Acad. Sci. USA *101*, 7158–7163.